transmission electron microscope. In the HREM image of a GaN nanorod with a diameter of about 14.9 nm (Fig. 5), the (100) fringes with the spacing of 0.276 nm are parallel to the edge of the nanorod.

In previous studies, GaN was prepared through the reaction $Ga_2O + 2NH_3 \rightarrow 2GaN + H_2O + 2H_2$; however, the products were GaN powders (*10*). This reaction was also conducted at 1173 K for 1 hour in our experimental setup. There were no nanorod products observed under TEM. Also, a reaction of carbon nanotubes and NH_3 was conducted at identical condition, which showed that the carbon nanotubes did not change in the absence of the Ga-Ga_2O mixture. These experimental results provide further support for the idea that the GaN nanorod products formed on the porous alumina plate through reaction 3.

Photoluminescence (PL) spectra of the GaN nanorods were measured in a Perkin-Elmer (Buckinghamshire, UK) LS50B fluorescence spectrophotometer with a Xe lamp at room temperature under 254-nm ultraviolet light excitation. The filter wavelength was 290 nm. The PL spectrum (Fig. 6) consists of one strong broad emission peak at 384 nm and another emission peak at 595 nm, which is similar to the PL spectra of GaN reported previously (*11*).

We also prepared Si_3N_4 nanorods using reaction 2 (*12*). The successful preparation of these nitride nanorods suggests that the method described in this report could be used to prepare a range of chemically distinct nitride nanorods, which might offer opportunities for both fundamental research and technological applications.

REFERENCES AND NOTES

1. S. Iijima, *Nature* **354**, 56 (1991).
2. S. Nakamura, M. Senoh, T. Mukai, *Appl. Phys. Lett.* **62**, 2390 (1993); S. N. Mohammad, A. Salvador, H. Morkoc, *Proc. IEEE* **83**, 1306 (1995).
3. Y. Xie, Y. Qian, W. Wang, S. Zhang, Y. Zhang, *Science* **272**, 1926 (1996); K. E. Gansalvaes, G. Carlson, S. P. Rangarajan, M. Benaissa, M. Joseyacaman, *J. Mater. Chem.* **6**, 1451 (1996); H. Yamane, M. Shimada, S. J. Clarke, F. J. Disalvo, *Chem. Mater.* **9**, 413 (1997).
4. H. Dai, E. W. Wong, Y. Z. Lu, S. Fan, C. Lieber, *Nature* **375**, 769 (1995).
5. W. Wong, B. W. Maynor, L. D. Burns, C. M. Lieber, *Chem. Mater.* **8**, 2041 (1996).
6. W. Han *et al.*, *Chem. Phys. Lett.* **265**, 374 (1997).
7. C. J. Frosch and C. D. Thurmond, *J. Phys. Chem.* **66**, 877 (1962).
8. Q. Li, S. Fan, W. Han, C. Sun, W. Liang, *Jpn. J. Appl. Phys. Part 2* **36**, L501 (1997).
9. The spread of diameters of the nanorods prepared on the basis of the carbon nanotubes has also been observed in preparing SiC nanorods [see (*6*)], where a simple model has been suggested to explain this phenomenon. The model may also be helpful in explaining the spread of diameters of the GaN nanorods.
10. C. M. Balkas and R. E. Davis, *J. Am. Ceram. Soc.* **79**, 2309 (1996).
11. T. Ogino and M. Aoki, *Jpn. J. Appl. Phys.* **19**, 2395 (1980); T. Atuki *et al.*, *Appl. Phys. Lett.* **67**, 2188 (1995); A. Argoitia *et al.*, *ibid.* **70**, 179 (1997).
12. Si_3N_4 nanorods were prepared through the reaction of carbon nanotubes with SiO under nitrogen (or ammonia) atmosphere at 1673 K for 1 hour. The reaction scheme can be expressed as $3SiO(g) + 3C(s) + 2N_2(g) \rightarrow Si_3N_4(s) + 3CO(g)$. The nanorods were 4 to 40 nm in diameter and up to 50 μm in length.

13. This work was supported by the Chinese National Foundation of Nature Science Research.

22 May 1997; accepted 14 July 1997

Corona Formation and Heat Loss on Venus by Coupled Upwelling and Delamination

Suzanne E. Smrekar* and Ellen R. Stofan

Coronae are volcanotectonic features that are unique to Venus and are interpreted to be small-scale upwellings. A model in which upwelling causes delamination at the edge of the plume head, along with deformation of a preexisting depleted mantle layer, produced the full range of topographic forms of coronae. If half of the coronae are active, delamination of the lower lithosphere could account for about 10 percent of Venus' heat loss, with another 15 percent due to upwelling. Delamination may occur in other geologic environments and could account for some of Venus' heat loss "deficit."

Venus is expected to be as geologically active as Earth because its size, mean density, and radioactive content indicate a comparable heat budget (*1*). The large and even distribution of unmodified impact craters suggests that Venus was geologically active until about 500 million years ago when activity apparently slowed (*2*). Critical questions for the evolution of Venus are what caused the decline in activity, how is Venus losing its heat, and why have Venus and Earth evolved so differently.

The tectonic style of a planet is defined by the mechanisms through which the hot, convecting interior, or mantle, transfers heat through the cold, stiff outer layer, called the thermal lithosphere. There are three geologically conventional end member methods of heat loss: hot spot volcanism, plate recycling (or plate tectonics), and lithospheric conduction (*1*). Hot spots, or surface manifestations of large-scale upwelling mantle plumes with broad (1000 to 2500 km) topographic rises, contribute only a small fraction (<5%) of Venus' heat budget (*3*). Data from the Magellan mission showed no evidence of global systems of spreading ridges, transform faults, and trenches that characterize terrestrial plate tectonics (*4*). Models of episodic heat loss (*5*), proposed to explain the apparent dearth of recent geologic activity, indicate that conduction through the lithosphere may currently be the dominant mechanism, but they do not actually predict the geologic signature of global overturn for comparison with observations. The thick lithosphere predicted by these models appears to be inconsistent with even a low level of ongoing volcanism and tectonism. The formation of coronae is consistent with a relatively thin lithosphere and may account for a significant portion of Venus' heat loss through small-scale mantle upwelling and recycling of the lower lithosphere through delamination.

Jet Propulsion Laboratory, California Institute of Technology, MS 183-501, 4800 Oak Grove Drive, Pasadena, CA 91109, USA.

*To whom correspondence should be addressed.

Coronae are nearly circular annuli of fractures and ridges (Fig. 1) that are interpreted as manifestations of small-scale mantle upwelling driven by thermal buoyancy (*6–8*). There are about 360 coronae on Venus, ranging in diameter from ~100 to 2600 km, with most in a diameter range of 200 to 400 km (*7*). Here we address many of the outstanding questions in the study of coronae, including why they are unique to Venus, how the full range of topographic profiles are produced, the relation between the topography and the annulus of fractures that characterize coronae, the subduction zone morphology found on the edges of some coronae (*9*), and the cause of their complex geologic history (*7*).

Initial studies of coronae from Magellan radar images defined five classes primarily on the basis of the shape of the annulus: concentric, asymmetric, multiple, radial/concentric, or concentric–double ring (*6*). The topographic shapes of the 360 coronae on Venus were classified into nine groups (*7*) (Table 1). Group 3 includes corona shapes such as an elevated rim surrounding a central dome (Fig. 1), two nested topographic rings, and partial annular rims with irregular interior topography.

Models of corona formation (*10–14*) predict a dome, plateau, or an elevated interior surrounded by a rim and an outer moat caused by relaxation of a plateau (groups 1 and 2 and some in group 3; about 25% of coronae). Koch and Manga (*15*) modeled the formation of a depression with an outer rim (group 4; 25% of coronae), where the depression forms as the rising thermal upwelling spreads out beneath the lithosphere. However, the models above predict only domes (*10, 11, 13, 14*), simplify the thermal and viscosity structure such that surface deformation may be overestimated (*15*), or require topographic relaxation of an initial steep plateau (*10, 12*). The shapes not predicted by previous models and the lack of evidence for a plateau stage at many coronae necessitate other explanations for corona formation.

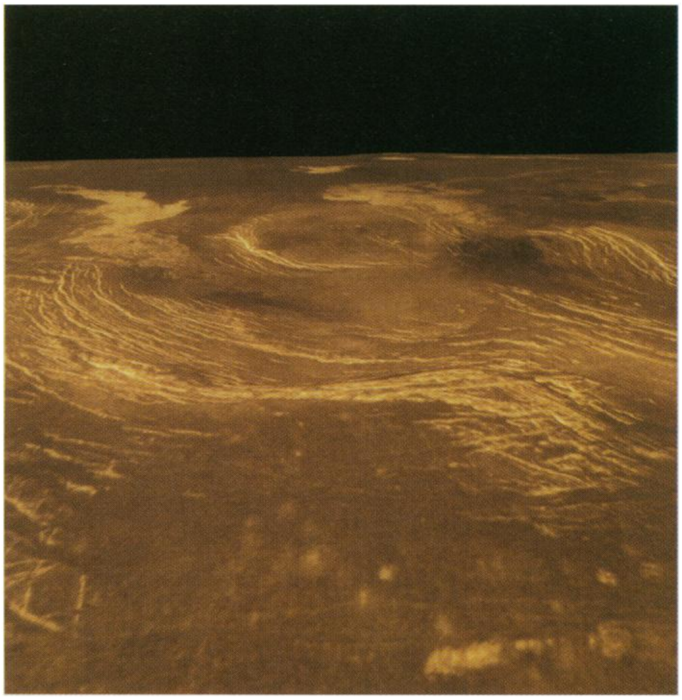

Fig. 1. Perspective image of Idem Kuva Corona, diameter 280 km. This corona has a raised rim and an inner dome-like structure and is the source of several long lava flows. The main portion of the fracture annulus lies along an elevated outer rim. A portion of an older, flooded annulus can be seen in the foreground (middle right), outside the current topographic rim. This image was produced by combining the Magellan radar image and altimetric data; the vertical exaggeration is 10×. The false color is based on images of the surface returned by Venera landers.

Table 1. Topographic groups. Vertical tick marks on topographic profiles indicate the typical location of annuli for each group.

Group	Topographic profile	Description	% of coronae
1		Dome	10
2	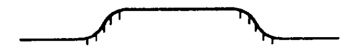	Plateau	10
3a		Rim surrounding interior high	21 (a+b)
3b		Rim surrounding interior dome	
4		Rim surrounding depression	25
5		Outer rise, trough, rim, inner high	5
6	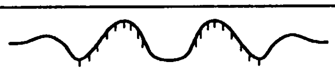	Outer rise, trough, rim, inner low	1
7		Rim only	7
8		Depression	7
9		No discernible signature	14

The annuli of coronae are also more complex than previously thought. First observations of coronae indicated that the annulus was composed of concentric compressional ridges (*16, 17*); later studies with Magellan data indicated that ridges are present, but extensional graben are more common (*6, 8*). Recent mapping studies indicate that some coronae may go through multiple stages of annulus formation (*17*). At several coronae, the topographic rim and the tectonic annulus do not coincide. At Idem Kuva Corona (Fig. 1), which belongs to group 3a, the older annulus segment lies outside the deformed, upraised rim (*17*). This annulus location and multiple phases of annulus formation are not predicted by prior models (*10–15*).

Coronae are not uniformly distributed on Venus (*6, 18*). They occur at hot spots (21%), along major rift zones (chasmata) or minor fracture belts (68%), and as relatively isolated features in the plains (11%) (*7*). Chasmata coronae generally formed coincident with extensional deformation (*7, 19*). The deep troughs around some coronae associated with chasmata have been interpreted as evidence for subduction (*9, 20*). Schubert and Sandwell (*9*) proposed that chasmata originate at the thinned lithosphere near hot spots; propagation of the rift into the cooler, thicker plains lithosphere results in foundering and subduction. They explain the circularity of coronae to be a coincidence of oppositely subducting arc segments and suggest that chasmata coronae have a fundamentally different origin than other coronae. However, coronae occur all along chasmata, including quite near and on hot spots, portions of the annular moats of chasmata coronae are not located along the chasmata, most coronae along chasmata are not surrounded by deep troughs, and all coronae are nearly circular. Also, some coronae in the plains and at hot spots are surrounded by deep annular moats. This, combined with the continuity of fractures across alleged subduction zones (*21*), suggests that an alternative explanation for trough formation should be sought.

If coronae formed by different mechanisms, one might expect distinct correlations between annulus shape, topography, and geologic setting (*22*). The only correlation between annulus shape and topography is that depressions with or without rims (groups 4 and 8) are almost exclusively concentric features. However, all other topographic groups also contain concentric coronae. In addition, no strong correlation exists between the annulus shape classes and geologic setting. The exception is the radial/concentric class, found only along chasmata (6, 7). The only topography–geologic setting correlation is between groups 7 (rim only) and 9 (little or no topography) and the plains setting. In other settings, a wide range of groups can be seen.

We carried out numerical experiments to investigate the effects of plume and lithospheric properties on corona formation (23). Our model predicts the time evolution of topography above a plume of finite duration that rises through the mantle, interacts with the lithosphere, and dies out when heat is no longer supplied from below (24). An axisymmetric finite difference scheme described temperature and chemistry variations, and a penalty function finite element formulation was used to solve the buoyant viscous flow equations (25). The viscosity was Newtonian, according to an Arrhenius form based on a dry olivine flow law (26), and was scaled to 10^{21} Pa/s at a mantle temperature of 1300°C. As our emphasis was on modeling the interaction of the plume with the lithosphere, we focused the computationally allowed temperature-dependent viscosity variation of 10^4 Pa/s in that region rather than distribute it over the entire area. In some models, a low-density layer of mantle residuum is included beneath the lithosphere and is assumed to be a result of prior melting events. We used a value of 20% depletion of Fe relative to Mg, consistent with the formation of a basaltic crust.

For the one case described in detail (Figs. 2 and 3), the initially 75-km-thick lithosphere thickens to ~195 km over the 400-million-year (My) duration of the calculation, and the mantle temperature decreases by ~20°C because heat is not continuously added to the system. A depleted mantle layer extends from the surface down to 150 km. The hot region at the base of the computational domain feeds the plume for 140 My. The plume reaches the lithosphere at ~100 My, and the plume tail rises for ~165 My. A dome forms as the plume uplifts the lithosphere (132 My) (Figs. 2 and 3). As the plume head spreads out and thins the lithosphere, the dome broadens. The dome subsides as the plume is shut off and begins to cool (196 My). The lithosphere thickens at the edge of the plume head as the plume spreads outward and downward (225 My). Sinking of the lower lithosphere, or delamination, pulls the surface downward. Delamination is driven initially by flow of the plume head and is sustained by the density difference between the lithosphere and mantle. Viscous flow pulls the delaminating lithosphere toward the center (246 My), shifting the surface trough. Eventually the trough merges into a central depression (278 My). The depleted mantle layer is pulled downward with the thermal lithosphere. The lowest topographic point is reached when the cold lithosphere pulling downward balances the low-density depleted layer pushing upward (304 My). As the depleted layer continues to thicken, the topography starts to increase (324 My). Continued thickening of the depleted layer causes a broad topographic ring to form at the center (392 My).

Other model runs with variations in the plume and lithospheric properties (23) predict somewhat different topographic forms (Table 2). Congestion of the delaminating ring as it moves inward can apply a torque on the ring causing a rim to form outside of the trough (groups 3 to 6, ~40% of coronae). For a very thick, depleted mantle layer, the initial effect when a plume encounters the layer is to cause a depression at the surface (group 8). For a depression to occur, the positive density anomaly due to thinning of the low-density residuum layer relative to the surrounding mantle must be greater than the negative density due to the hot plume. A dome can eventually form at the center of the depression if the plume persists (group 1). If delamination develops and the temperature difference in the lithosphere dissipates before the delaminating lithosphere reaches the center of the corona, isostatic rebound of the depleted mantle creates a ring of high topography (group 7).

Our model predicts all of the corona groups (Table 2). Groups 3 to 6 can be produced as a result of early stage delamination, and groups 7 to 9 can be produced as late stage phases of delamination. Deformation of a depleted mantle layer can produce the interior depressions seen in topographic groups 3b, 4, 5, 6, and 8. Only isostatic rebound of a depleted mantle layer pulled down by delamination produces topographic group 7. This process could also be responsible for some of the rims and rises seen in groups 3 to 6. Groups 5 and 6 (6% of coronae) have only been produced at larger scales (2000-km diameter). It is possible that these forms require a larger ratio of plume diameter to lithospheric thickness than for the cases shown. The implication may be that these forms require a thinner lithosphere.

In addition to predicting the observed topography, the model predictions are consistent with studies of the geologic history of coronae and their general geologic setting. The predicted evolution of the topography is complex, consistent with the observation that coronae topographic highs and fracture annuli do not always coincide.

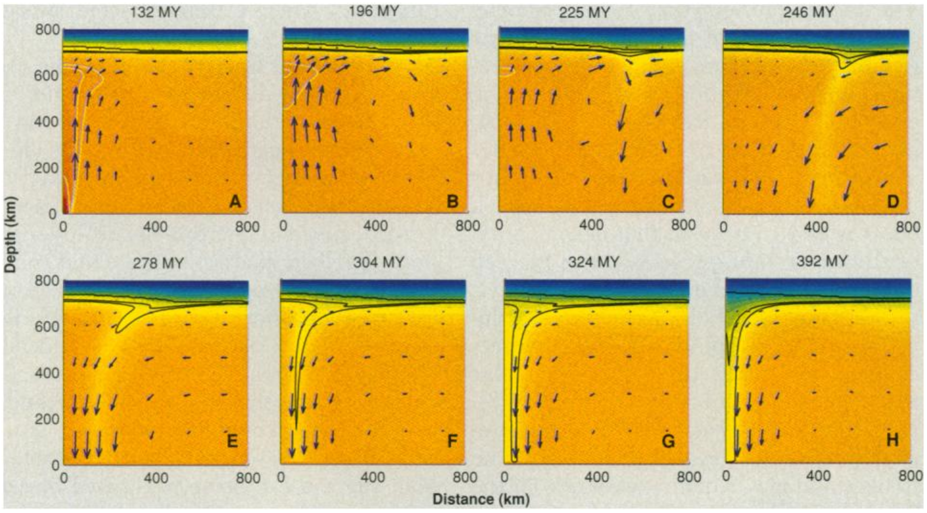

Fig. 2. (**A** to **H**) Time evolution of the temperature, composition, and flow fields. Arrows indicate the direction and relative magnitude of the viscous flow. Temperature is shown with color, with blue cold and red hot. White contours are at 1325°C, 1350°C, and 1500°C. Depletion at 1, 5, and 10% is shown with black contours. The 1% contour is the lowermost line.

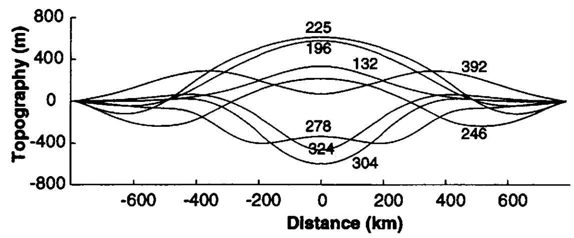

Fig. 3. Topography for the same time steps as illustrated in Fig. 2. Note that the topography is reflected about the vertical axis to show the entire profile across the upwelling, contrary to Fig. 2 where the computational domain is shown without reflection.

The model predicts that the topography continues to evolve long after the plume thermal anomaly has dissipated, in agreement with observations suggesting a long evolution (*17, 27*). In addition, the topography and position of the fracture annulus at many coronae varies azimuthally. This irregularity is not predicted by our model, but it is easy to imagine that delamination of the lower lithosphere will not proceed uniformly toward the center for geometric reasons. The model also provides an explanation for topographic troughs as a direct consequence of upwelling and is consistent with estimates of limited convergence (*28*). However, the viscous model does not predict the observed steep relief of some of the troughs and may require a weakness in the lithosphere that allows it to break and be more readily pulled downward, such as a rift (*9*).

We interpret the model predictions and geologic observations as evidence of a depleted mantle layer. The isostatic rebound of a depleted mantle layer pulled downward by delamination is the only model that predicts group 7. This formation mechanism is consistent with the observation that rim formation is a late stage event (*17*). Additional evidence in favor of the presence of a depleted mantle layer is the predominance of coronae having only a rim (group 7) and coronae with little topographic relief (group 9) in plains regions. A thicker depleted mantle layer is expected beneath the relatively stable plains regions, just as on Earth a chemical lithosphere is believed to occur beneath continents (*29*). Further, the correlation between topographic depressions and concentric coronae and the observation that many of these coronae have no radial fractures suggest that central uplift may not occur at all coronae. The correlation between a chasmata setting and the radial/concentric class may indicate a lack of depleted mantle at rifts zones, where a thin, depleted layer is expected.

Model results indicate that inferring specific plume or lithospheric properties or even the evolutionary stage of a corona is not straightforward. In general, the more complex the deformation and topography, the later the stage of evolution. Geologic history can aid in inferring the evolutionary stage. Geologic analyses indicate that annulus shape, topography, and geologic setting of coronae are not well correlated. We interpret this lack of correlation as evidence that corona evolutionary stage is usually more important than lithospheric thickness in determining corona morphology.

The contribution to planetary cooling from coronae can be approximated by calculating the buoyancy flux due to the temperature difference between the delaminating ring or plume and the surrounding mantle. Buoyancy flux is defined as Mv, where M is mass per unit area and v is velocity. The mass is given by $\rho\alpha\Delta T$, where ρ is the reference mantle density (3300 kg/m^3), α is the coefficient of thermal expansion (3×10^{-5} K^{-1}), and ΔT is the temperature. The buoyancy flux for the plume (Fig. 2A) at a depth of 600 km below the surface is 2.1 Mg/s. The buoyancy flux of the delaminating lithosphere at a depth of 400 km (Fig. 2D) is 3.0 Mg/s. The 800-km diameter of the model corona (Figs. 2 and 3) is larger than the average corona diameter of about 300 km (*6*). Because the cross-sectional area is proportional to the square of the radius, the average corona buoyancy flux should be a factor of $300^2/800^2$ smaller, or 0.30 Mg/s for the plume and 0.42 Mg/s for the delaminating lithosphere.

The overall contribution by coronae to planetary heat loss is difficult to estimate because their current level of activity is uncertain. Analysis of crater densities suggests that coronae range in age from 0 to ~350 My (*30*), and mapping studies suggest that many coronae are sites of persistent geologic activity over time (*17, 27*). To estimate the number of active coronae, we assumed that those coronae that have a raised interior (~180 of the 360 coronae) are active because a thermal anomaly is likely to be present under most domes. This may be a conservative estimate, because our model does not require dome-shaped topography at active features. Of these coronae, about half have an outer rim, which could be a result of delamination. If both plumes and delamination are active, this gives a buoyancy flux estimate of 90 coronae $\times$ 0.72 Mg/s = 65 Mg/s. If another 90 coronae have active plumes but are not delaminating, the additional flux would be 90 $\times$ 0.30 Mg/s = 27 Mg/s.

A precise estimate of buoyancy flux for plumes is difficult because of uncertainties in plume, lithospheric, and mantle properties even for terrestrial hot spots (*31*), where better constraints are available than for Venus. However, we believe the estimate we present is a reasonable, if not lower, bound because of the long plume duration assumed. The longer the duration of the plumes, the lower the buoyancy flux required to create a given topographic height. We have estimated the buoyancy flux using a plume lasting 140 My in which the corona topography continues to evolve for at least 275 My. Considerably longer evolution times are probably unlikely, given the resurfacing age of the planet of ~500 My (*2*) and indications that coronae are relatively young features (*30*). Using a model of a cooling thermal diapir, Musser and Squyres (*14*) found lifetimes of tens to hundreds of millions of years.

The estimated buoyancy flux for terrestrial hot spots is ~50 Mg/s, which accounts for about 10% of the total planetary heat flux of ~82 mW/m^2 (*32*). Heat flux for Venus is a matter of debate, but typical estimates range from 35 to 65 mW/m^2 (*33*). On the basis of the higher end of this range, which is appropriate for our models that assume an Earth-like lithospheric thickness, coronae could account for as much as ~25% of the heat flux on Venus.

Delamination in other geologic environments, such as highland plateaus, could also play a role. Competing theories for their origin are upwelling and downwelling (*34, 35*). For prior downwelling models, the time scale of deformation was prohibitively long (*35*). The mechanism of coupled upwelling and delamination proposed here for corona formation may be able to explain more of the characteristics of highland plateau formation than prior models. The final plateau in this model would be a result of isostatic rebound of residuum material pulled downward by delamination. The general geologic

Table 2. Corona topographic element formation mechanisms.

Topographic elements	Formation mechanisms
	Interior forms
Dome	Uplift by hot plume.
	Isostatic uplift of a depleted mantle layer thickened by delamination.
Depression	Late-stage isostatic adjustment of thinned lithosphere.
	Early-stage thinning of depleted mantle layer.
	Suction above delaminating ring migrating toward interior.
Plateau	Relaxation of dome above cooling plume.
No relief	Thinning of depleted layer.
	Final stage of thermal equilibration after plume cools.
	Exterior forms
Outer rim	Isostatic rebound of depleted material after delaminating ring equilibrates.
	Viscous relaxation of plateau.
	Congestion of delaminating ring.
Trough	Suction above delaminating ring.

history implied by plateau formation through coupled upwelling and delamination appears consistent with the observed structures at some highland plateaus (*36*). This concept must be demonstrated numerically, but it serves to illustrate one possible example of coupled upwelling and delamination in addition to coronae, indicating the potential significance of this process for heat loss on Venus.

The success of our model in explaining why coronae are unique to Venus and in predicting topographic forms and a long, complex deformation history provides an indication that delamination of the lower lithosphere and deformation of a depleted mantle layer are likely to be occurring on Venus. The overall picture of Venus suggested by these results is one in which a significant amount of heat is lost by delamination of the lower lithosphere and small-scale upwellings. In the absence of large-scale, linear upwellings at ridges and downwellings at subduction zones that characterize terrestrial plate tectonics, small-scale upwellings and delamination may accomplish the same heat loss but result in less disruption of the surface and lower resurfacing rates. On Earth, surface deformation is predominantly a result of large-scale lateral translation of plates, which involves deformation of the entire lithosphere. The surface deformation due to vertical motions at hot spots and possible delamination sites is far more subtle and does not result in resurfacing of the entire region uplifted. For example, at hot spot swells on Earth, resurfacing by volcanism and extension affects only a small fraction of the entire area uplifted. The large resurfacing age on Venus has been interpreted to indicate a thick thermal lithosphere (*5*, *37*). Here we suggest it is simply a result of a different tectonic style. Our results indicate that a thin (~100 km thick) lithosphere may be consistent with both low resurfacing rates and high heat flow. In addition, these results suggest that coronae with typical diameters of several hundred kilometers are inconsistent with lithospheric thicknesses significantly greater than 100 km, consistent with other corona models (*12*, *38*).

The issue of whether or not a change in the style or rate of geologic processes on Venus is required by the crater distribution remains open. Recent work suggests that resurfacing of much of the planet may not have occurred catastrophically but rather over a period of 500 My (*39*). If widespread lithospheric overturn did occur on Venus, as suggested to explain the resurfacing history (*5*), such an event could have aided the loss of water from the mantle and the associated mantle-lithospheric decoupling. The loss of a low-viscosity zone might have caused a transition from a more Earth-like style of plate tectonics in which the entire lithosphere is free to deform to one in which a strongly coupled lithosphere and mantle effectively confine the most vigorous deformation to the lower lithosphere (*40*).

The importance of strong coupling between the lithosphere and mantle (in the absence of a water-related low-viscosity zone beneath the lithosphere) in these results furthers the argument that water may be the primary factor shaping the differing tectonic styles of Venus and Earth (*41*) and presents an explanation for why coronae are unique to Venus. The mechanism of coupled upwelling and downwelling may also be relevant to the problem of the driving force for initiation of subduction (*42*). There is evidence supporting a hotter lithosphere and a dehydrated upper mantle in the Archean (*43*), the earliest period of Earth's geologic history, which suggests that strong coupling of the mantle and lower lithosphere may have occurred.

REFERENCES AND NOTES

1. S. C. Solomon and J. W. Head, *J. Geophys. Res.* **87**, 9236 (1982).
2. R. J. Phillips *et al.*, *ibid.* **97**, 15923 (1992).
3. S. E. Smrekar and E. M. Parmentier, *ibid.* **101**, 5397 (1996).
4. S. C. Solomon *et al.*, *Science* **252**, 297 (1991).
5. E. M. Parmentier and P. C. Hess, *Geophys. Res. Lett.* **19**, 2015 (1992); D. L. Turcotte, *J. Geophys. Res.* **98**, 17061 (1993).
6. E. R. Stofan *et al.*, *J. Geophys. Res.* **97**, 13347 (1992).
7. E. R. Stofan, V. E. Hamilton, D. M. Janes, S. E. Smrekar, in *Venus II*, S. W. Brougher, D. M. Hunten, R. J. Phillips, Eds. (Univ. of Arizona Press, Tucson, AZ, 1997), pp. 931–965.
8. S. W. Squyres *et al.*, *J. Geophys. Res.* **97**, 13611 (1992).
9. G. Schubert and D. T. Sandwell, *Icarus* **117**, 173 (1995).
10. E. R. Stofan, D. L. Bindschadler, J. W. Head, E. M. Parmentier, *J. Geophys. Res.* **96**, 20933 (1991).
11. D. M. Janes *et al.*, *ibid.* **92**, 16055 (1992).
12. D. M. Janes and S. W. Squyres, *ibid.* **100**, 21173 (1995).
13. D. M. Koch, *ibid.* **99**, 2035 (1994).
14. G. S. Musser Jr. and S. W. Squyres, *ibid.* **102**, 6581 (1997).
15. D. M. Koch and M. Manga, *Geophys. Res. Lett.* **23**, 225 (1996).
16. V. L. Barsukov *et al.*, *J. Geophys. Res.* **91**, 378 (1986); A. A. Pronin and E. R. Stofan, *Icarus* **87**, 452 (1990).
17. D. L. Copp, J. E. Guest, E. R. Stofan, in preparation.
18. S. W. Squyres *et al.*, *Geophys. Res. Lett.* **20**, 2965 (1993).
19. V. E. Hamilton and E. R. Stofan, *Icarus* **121**, 171 (1996).
20. D. T. Sandwell and G. Schubert, *Science* **257**, 766 (1992).
21. V. L. Hansen and R. J. Phillips, *ibid.* **260**, 526 (1993).
22. One hypothesis might be that isolated plains coronae form through delamination (peeling away of the lower lithosphere as a result of density instabilities) and coronae along chasmata are upwellings. Conversely, if coronae all form by the same mechanism, differences in the morphologic characteristics of coronae between each geologic setting may provide constraints on regional lithospheric structure. For instance, the lithosphere along rifts or at hot spots might be thinner than in the plains.
23. A series of 12 numerical cases were run in which plume and lithospheric parameters were varied. Delamination of the lower lithosphere developed in half of these cases. The initial temperature and width of the hot region at the base of the computational domain was varied from 1750°C to 2200°C and 50 to 100 km, respectively. The plume duration was varied from 50 to 430 My. The base of the high-viscosity thermal lithosphere is defined as the 1100°C contour. The lithospheric thickness range was 50 to 150 km; the range of residuum layer thickness was 0 to 200 km, where the thickness is counted as starting at the surface. The radial and vertical dimensions of the computational domain were varied from 250 to 800 km. In addition to these 12 cases, more than 50 cases were run with a radius of 2400 km. These cases were aimed at modeling large-scale hot spot–like features; 15 of these were reported on in (3). As noted in Table 1, a few of the corona topographic groups have only been predicted to date in the larger scale numerical models.
24. The upwelling arises from a "hot patch" that consists of a high-temperature region at the base of the central axis of the computational domain in which temperature decreases linearly away from the axis. There was no attempt to match the depth of the box to a physical boundary such as the core-mantle boundary. Rather, the computational resources were devoted to modeling the top of the convecting boundary layer (that is, the lithosphere). Indeed, the origin of upwellings that create coronae is unknown, but it is believed to lie in the upper mantle on the basis of coronae size. There are no rigorous constraints on the duration of plumes on Venus. The maximum duration of plumes on Earth is also poorly constrained because of destruction of the lithosphere, but the oldest probable plume is 200 My [R. White and D. P. McKenzie, *J. Geophys. Res.* **94**, 7685 (1989)]. Thus the range of plume duration was chosen to be comparable to that of terrestrial plumes while allowing for a large variation. In trying to model plumes that fit the observed range of topography, plume temperature (and thus buoyancy) trades off with plume duration. Again, the temperature of terrestrial plume heads when they reach the base of the lithosphere was used as a guide, with a typical peak temperature when the plume encounters the lithosphere of ~1390°C or higher.
25. The finite element grid was 90 by 90 elements; the finite difference grid had twice as many elements. The element spacing was nonuniform to give maximum resolution in the axial upwelling region and in the region where the plume interacts with the lithosphere. The vertical normal stress and shear stress were assumed to vanish at the bottom boundary and at the vertical outer boundary of the cylindrical domain. Boundary conditions were rigid (vanishing horizontal and vertical velocity) at the top of the cylindrical region. The surface and interior temperatures were 500° and 1300°C, respectively. Nondiffusing chemical variations were calculated with a particle-in-cell type method [K. Jha, E. M. Parmentier, J. Phipps Morgan, *Earth Planet. Sci. Lett.* **125**, 221 (1994)]. More details of the numerical approach are given in (3) and references therein.
26. S. I. Karato, M. S. Paterson, J. D. Fitzgerald, *J. Geophys. Res.* **96**, 20947 (1991).
27. E. R. Stofan and J. E. Guest, *Lunar Planet. Sci.* **XXVII**, 1277 (1996).
28. C. D. Brown and R. E. Grimm, *Icarus* **117**, 219 (1995).
29. T. H. Jordan, special issue on the International Conference on Oceanic and Continental Lithosphere; Similarities and Differences, *J. Petrol.* **1988**, 11 (1988).
30. M. Price and J. Suppe, *Nature* **372**, 756 (1994).
31. S. Stein and C. A. Stein, *Science* **275**, 1613 (1997).
32. G. F. Davies, *Earth Planet. Sci. Lett.* **123**, 277 (1992).
33. R. J. Phillips *et al.*, in *Venus II*, S. W. Brougher, D. M. Hunten, R. J. Phillips, Eds. (Univ. of Arizona Press, Tucson, AZ, 1997), pp. 1163–1204.
34. D. L. Bindschadler and E. M. Parmentier, *J. Geophys. Res.* **95**, 21329 (1990); R. J. Phillips, R. E. Grimm, M. C. Malin, *Science* **252**, 651 (1991).

35. J. G. Kidder and R. J. Phillips, *J. Geophys. Res. (Planets)* **101**, 23181 (1996); A. Lenardic, D. M. Koch, W. M. Kaula, D. L. Bindschadler, *ibid.* **100**, 16949 (1995).
36. V. L. Hansen and R. J. Phillips, *Geology* **23**, 292 (1995).
37. S. C. Solomon, *Phys. Today* **46**, 48 (1993); W. B. Moore and G. Schubert, *Geophys. Res. Lett.* **22**, 429 (1995); V. S. Solomatov and L.-N. Moresi, *J. Geophys. Res.* **101**, 5397 (1996).
38. K. E. Cyr and H. J. Melosh, *Icarus* **102**, 175 (1993).
39. S. A. Hauck II, R. J. Phillips, M. Price, *Lunar Planet. Sci. Conf.* **XXVIII**, 527 (1997).
40. R. J. Phillips, W. M. Kaula, G. E. McGill, M. C. Malin, *Science* **212**, 879 (1981).
41. W. M. Kaula, *Geophys. Res. Lett.* **17**, 1401 (1990); *Science* **270**, 1460 (1995); R. J. Phillips, *J. Geophys. Res.* **95**, 1301 (1990).
42. S. Mueller and R. J. Phillips, *J. Geophys. Res.* **96**, 651 (1991).
43. P. H. Warren, *Geology* **12**, 335 (1984).
44. We thank M. Parmentier for the use of his numerical code and J. Hall and E. DeJong for their assistance in creating the Magellan topography and image overlay. Supported by NASA Planetary Geology and Geophysics Program grants 151-01-70-71 to S.E.S. and 151-01-70-59 to E.R.S. The Jet Propulsion Laboratory–Caltech Cray Supercomputer used in this investigation was provided by funding from the NASA Offices of Mission to Planet Earth, Aeronautics, and Space Science. The research presented in this report was carried out at the Jet Propulsion Laboratory, California Institute of Technology, under a contract with NASA.

23 April 1997; accepted 11 July 1997

Bipolar Changes in Atmospheric Circulation During the Little Ice Age

K. J. Kreutz,* P. A. Mayewski, L. D. Meeker, M. S. Twickler, S. I. Whitlow, I. I. Pittalwala

Annually dated ice cores from Siple Dome, West Antarctica, and central Greenland indicate that meridional atmospheric circulation intensity increased in the polar South Pacific and North Atlantic at the beginning (~1400 A.D.) of the most recent Holocene rapid climate change event, the Little Ice Age (LIA). As deduced from chemical concentrations at these core sites, the LIA was characterized by substantial meridional circulation strength variability, and this variability persists today despite strong evidence for an end to LIA cooling. Thus, increased late 20th century storm variability may be in part a result of the continuation of these climatic fluctuations.

The LIA (nominally ~1400 to 1900 A.D.) is recorded in several Northern Hemisphere and equatorial paleoclimatic records; it was a period of cold, dry conditions and increased atmospheric circulation (*1–4*). It now appears that several LIA-type events have occurred throughout the Holocene (*2*) and that relatively minor forcings may be responsible for these events (*5*).

Although it was a globally distributed event, the LIA was not a 500-year period of global cooling. High-resolution tree ring records from several areas (*6*) have suggested that although there is substantial decadal-scale variability related to temperature changes over the last 2000 years, no distinct LIA signal is recorded. Indeed, it is possible that the LIA was not simply a cooling everywhere but instead a period of both warm and cold anomalies that varied in importance geographically (*7*). Such patterns can be attributed to changes in atmospheric circulation strength (*8*). Although instrumental records of atmospheric circulation strength do not encompass the entire LIA period, ice-core glaciochemical records can provide a proxy for this climate parameter (*2*). Here we present results of annually dated, multivariate chemical records from a new ice core at Siple Dome, West Antarctica, and the previously described Greenland Ice Sheet Project Two (GISP2) (*2*) ice core that allow a comparison of changes in regional atmospheric circulation in the South Pacific and North Atlantic, respectively, throughout the last 1150 years (Fig. 1).

Siple Dome (81.654°S, 148.808°W; Fig. 1) is sensitive to changing coastal meteorological conditions because of its low elevation (621 m) and because many cyclones pass across the relatively flat Ross Ice Shelf to the site (*9, 10*). In 1994, a 150-m ice core was collected 5 km north of the Siple Dome summit (*10*). Annual layers are evident in the core (*11*), and ice with an age of 1150 years before the present (2000 A.D.) is present at a depth of 150 m (the dating error is estimated to be ~1%). The average accumulation rate is 13.3 cm of ice equivalent per year.

The concentrations of sea-salt species (namely, Na^+, Cl^-, Mg^{2+}, and K^+) in Antarctic and Greenland surface snow decrease exponentially with both distance inland and elevation because coarse mode sea-salt aerosols fall out of the air during transport (*10, 12*). Therefore, changes in the concentration of these species in the ice core imply fluctuations in the frequency and intensity of tropospheric aerosol transport to a particular site (*10, 12*). Sea-salt deposition occurs at Siple Dome primarily during the austral winter when cyclonic frequency is at a maximum (*9*). Fluctuations in the position and intensity of the Amundsen Sea Low (ASL) in response to atmospheric heating over the Pacific Ocean (*9*) are likely linked to Siple Dome glaciochemistry on interannual time scales. On longer time scales (decades to centuries), overall expansion (deepening) of the ASL associated with changes in the latitude of the Antarctic low-pressure belt, and hence the southern circumpolar vortex extent (*9*), is most likely responsible for increased aerosol transport. Similarly, in central Greenland, most sea salt is deposited in the boreal winter when the meridional air flow is intensified and the northern polar vortex is expanded (*2, 13*). Enhanced winterlike meteorological conditions in the South Pacific and North Atlantic therefore appear to be consistent with increased sea-salt concentrations at both of these sites. Na^+ is the most conservative sea-salt species in the Siple Dome and GISP2 records (*14*) and therefore provides the best single-species representation of changing sea-salt aerosol concentration.

The onset of LIA conditions in the GISP2 Na^+ record at ~1400 A.D. is abrupt [within ~20 years (*2*)] (Fig. 2). The record implies that this was the most dramatic change in atmospheric circulation (*2*) and surface temperature conditions (*15*) in the last 4000 years. Siple Dome Na^+ values also began to increase above the 1150-year mean at ~1400 A.D. (*16*). It appears (Fig. 2) that LIA conditions began ~28 years earlier at Siple Dome than at GISP2 (*16*). This offset is close to the combined dating error of the two records at that depth (estimated to be 12 to 20 years). Therefore, although it is possible that the difference is real, we conclude that changes in atmospheric circulation occurred abruptly and synchronously in the South Pacific and North Atlantic at ~1400 A.D.

Both the Siple Dome and GISP2 Na^+ records contain significant decadal-scale variability during the LIA. It appears that regional atmospheric circulation fluctuations were of similar magnitude and timing in both polar hemispheres (*16*). In particular, from 1680 to 1730 A.D., Na^+ concentrations were high in both records. During

K. J. Kreutz and P. A. Mayewski, Climate Change Research Center, Institute for the Study of Earth, Oceans, and Space and Department of Earth Sciences, University of New Hampshire, Durham, NH 03824, USA.
L. D. Meeker, Climate Change Research Center, Institute for the Study of Earth, Oceans, and Space, and Department of Mathematics, University of New Hampshire, Durham, NH 03824, USA.
M. S. Twickler, S. I. Whitlow, I. I. Pittalwala, Climate Change Research Center, Institute for the Study of Earth, Oceans, and Space, University of New Hampshire, Durham, NH 03824, USA.

*To whom correspondence should be addressed. E-mail: karl.kreutz@unh.edu